



Femtosecond Response of Quasiparticles and Phonons in Superconducting $\text{YBa}_2\text{Cu}_3\text{O}_{7-\delta}$ Studied by Wideband Terahertz Spectroscopy

A. Pashkin,¹ M. Porer,¹ M. Beyer,¹ K. W. Kim,^{1,2} A. Dubroka,² C. Bernhard,² X. Yao,³ Y. Dagan,⁴ R. Hackl,⁵ A. Erb,⁵ J. Demsar,^{1,6} R. Huber,^{1,*} and A. Leitenstorfer¹

¹*Department of Physics and Center for Applied Photonics, University of Konstanz, 78457 Konstanz, Germany*

²*Department of Physics, University of Fribourg, 1700 Fribourg, Switzerland*

³*Department of Physics, Shanghai Jiao Tong University, Shanghai 200240, China*

⁴*Raymond and Beverly Sackler School of Physics and Astronomy, Tel Aviv University, Tel Aviv, 69978, Israel*

⁵*Walther-Meissner-Institut, 85748 Garching, Germany*

⁶*Complex Matter Department, Jozef Stefan Institute, Ljubljana, Slovenia*

(Received 3 May 2010; published 2 August 2010)

We measure the anisotropic midinfrared response of electrons and phonons in bulk $\text{YBa}_2\text{Cu}_3\text{O}_{7-\delta}$ after femtosecond photoexcitation. A line shape analysis of specific lattice modes reveals their transient occupation and coupling to the superconducting condensate. The apex oxygen vibration is strongly excited within 150 fs, demonstrating that the lattice absorbs a major portion of the pump energy before the quasiparticles are thermalized. Our results attest to substantial electron-phonon scattering and introduce a powerful concept probing electron-lattice interactions in a variety of complex materials.

DOI: 10.1103/PhysRevLett.105.067001

PACS numbers: 74.72.-h, 74.25.Kc, 78.47.jg

The interaction of electrons with the crystal lattice represents one of the most elusive yet pivotal aspects of high-temperature superconductors (HTSCs). Although purely phonon-mediated BCS-type pairing fails to explain essential properties of superconducting (SC) cuprates, convincing evidence of significant electron-phonon contributions has been provided by angle-resolved photoemission [1–3], inelastic neutron scattering [4], tunneling [5], and Raman [6] spectroscopies. For time-integrated techniques it is difficult, however, to disentangle the interplay between elementary excitations.

Pump-probe studies have been harnessed to establish a temporal hierarchy of microscopic interaction processes in HTSCs following a strong optical perturbation. Near-infrared [7,8], midinfrared [9], and terahertz (THz) probe pulses [10] as well as Raman scattering [11] have been employed to study the recombination of photoexcited quasiparticles (QPs) and the recovery of the SC condensate. A recent time-resolved photoemission study of $\text{Bi}_2\text{Sr}_2\text{CaCu}_2\text{O}_{8+\delta}$ has analyzed the relaxation of the quasiequilibrium electronic temperature assuming a selective electron-phonon coupling [12]. However, since these experiments do not directly monitor the lattice degrees of freedom themselves, a more detailed picture of the role of the various phonon modes during an initial nonthermal regime has been beyond reach. Ultrafast electron diffraction has fuelled the hope to follow the evolution of the lattice directly [13], yet the time resolution has been limited to the picosecond scale so far.

Here we report a direct and simultaneous observation of QP and phonon resonances on the same femtosecond scale. Multi-THz few-cycle pulses monitor the midinfrared conductivity of optimally doped $\text{YBa}_2\text{Cu}_3\text{O}_{7-\delta}$ (YBCO) as a function of the delay time τ after a near-infrared excitation

by 12-fs pulses. The resonant probe simultaneously traces the signatures of the SC gap, QP excitations, and two specific phonon modes. The dynamics of the phonon line shapes allows us to monitor vibrational occupations with a femtosecond resolution and to single out the coupling to the SC order parameter. We show that hot phonon effects and the creation of QPs both occur within 150 fs. This fact indicates extremely fast electron-phonon scattering in YBCO, in contrast to the usual assumption of a two-temperature model [14,15].

Optimally doped single crystals of YBCO ($T_c = 92$ K) form a prime laboratory for unconventional superconductivity. All measurements are carried out on as-grown surfaces oriented along or normal to the c axis of the twinned system [16,17]. As seen in the insets in Fig. 1, the direction of the probe field \mathbf{E} may be chosen either parallel or perpendicular to c . Figure 1(a) shows the real part of the in-plane conductivity ($\mathbf{E} \perp c$) in the normal and SC states, measured by ellipsometry [18]. As the temperature is decreased below T_c , σ_1 drops sharply at energies $\hbar\omega < 110$ meV due to the opening of a SC gap [19]. A Drude-like contribution dominates the low-energy edge of the response even at $T = 10$ K, as expected for a d -wave order parameter where nodal QPs exist at finite temperatures. According to oscillator sum rules, the spectral weight defined by the highlighted area in Fig. 1(a) is proportional to the density of condensed QPs [19].

While the in-plane response is dominated by electronic excitations, their contribution to the interplane optical conductivity ($\mathbf{E} \parallel c$) is reduced by 1 order of magnitude [see Fig. 1(b)]. This is why two phonon modes of B_{1u} symmetry appear prominently on top of the electronic background: (i) The narrow resonance at $\hbar\omega = 39$ meV is caused by Cu-O bond bending involving an in-phase

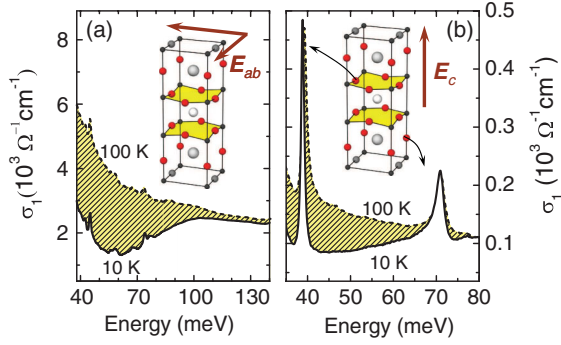


FIG. 1 (color). Optical conductivity $\sigma_1(\omega)$ of YBCO in the SC ($T = 10$ K, solid curve) and normal ($T = 100$ K, broken curve) states for (a) $\mathbf{E} \perp c$ and (b) $\mathbf{E} \parallel c$. Insets: Unit cell of YBCO and directions of the probe electric field. The oxygen ions involved in the observed vibrations are shown in red. The modes centered at 39 and 71 meV in (b) correspond to the bond-bending and apex oxygen vibrations, respectively.

motion of all oxygen ions within the cuprate bilayers. (ii) Collective vibrations of the apical oxygen ions located between the bilayers and the chains account for the conductivity maximum centered at $\hbar\omega = 71$ meV [20]. The bond-bending mode displays an anomalous blueshift and a slight broadening [Fig. 1(b)] as the system is heated towards T_c [21–24]. At the same time, the apex line changes from an asymmetric shape in the SC state to an almost symmetric one above T_c [22]. The origin of this effect will be discussed in more detail below.

In order to disentangle the ultrafast interplay between electrons and lattice, we perturb the SC state optically and trace the induced transition to the normal state with multi-THz transients. Details about our experimental setup are given in Ref. [17]. The unique stability of our laser system allows us to pursue, for the first time, field-sensitive reflection studies in bulk, single-crystalline YBCO of arbitrary orientation. The measured transient reflectivity provides direct access [25,26] to the pump-induced changes of the complex conductivity spectra, $\Delta\tilde{\sigma}(\omega, \tau) = \Delta\sigma_1(\omega, \tau) + i\Delta\sigma_2(\omega, \tau)$, as a function of energy and the time delay τ , without a Kramers-Kronig transform.

Figure 2(a) and 2(b) depicts the ultrafast response at a base temperature of $T = 20$ K. The excitation fluence of $\Phi \approx 0.3$ mJ/cm² is chosen to exceed the saturation threshold required to suppress superconductivity [17,27]. We first discuss the transient in-plane response mapped out in Fig. 2(a). The pump pulse barely affects the high energy part of the conductivity, whereas $\sigma_1(\omega)$ is enhanced below $\hbar\omega \approx 110$ meV due to the contribution of photogenerated QPs. The absolute size and the spectral shape of the pump-induced signal correspond to the conductivity difference between the SC and normal states [Fig. 2(c)]. The time evolution of the change of the spectral weight, $S_{\text{QP}} = \int \Delta\sigma_1(\omega, \tau) d\omega$, between 40 and 130 meV is shown in Fig. 2(d). Interestingly, S_{QP} reaches its maximum with a delay of 150 fs, distinctly slower than our time resolution

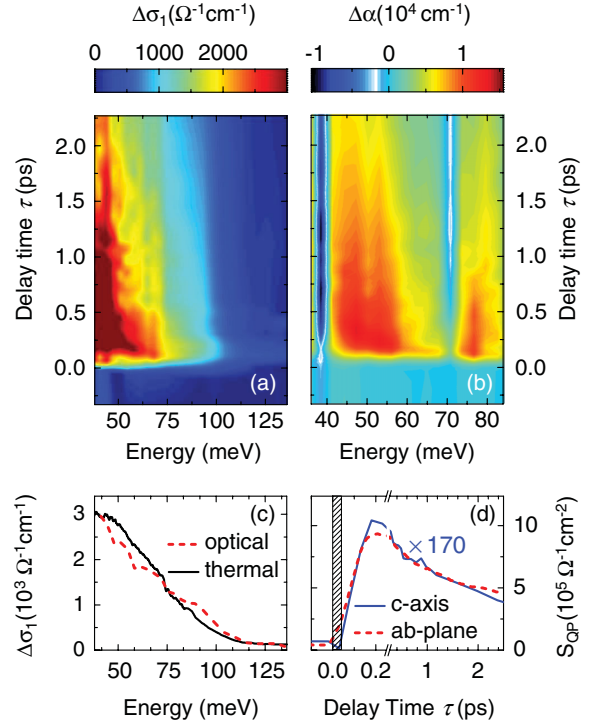


FIG. 2 (color). 2D optical pump-THz probe data: (a) Pump-induced changes $\Delta\sigma_1(\omega, \tau)$ as a function of the photon energy and the pump delay time τ , for $\mathbf{E} \perp c$. (b) Corresponding changes of $\Delta\alpha(\omega, \tau)$, for $\mathbf{E} \parallel c$. Both experiments are performed at $T = 20$ K with $\Phi = 0.3$ mJ/cm². (c) Conductivity difference between normal and SC states (solid curve) for $\mathbf{E} \perp c$ and pump-induced $\Delta\sigma_1(\omega, \tau)$ at delay time $\tau = 1$ ps after photoexcitation (broken curve). (d) Dynamics of the photoinduced QP spectral weight as a function the delay time τ . Dashed curve: Spectral weight for $\mathbf{E} \perp c$ integrated between 40 and 130 meV. Blue line: Spectral weight (scaled by factor 170) for $\mathbf{E} \parallel c$ between 45 and 60 meV. The experimental time resolution is indicated by the hatched area.

of 40 fs. These data present the first direct observation of the QP density generated during the pair-breaking cascade on the inherent time scale. The subsequent decay is described well by two exponential functions with time constants of 0.4 and 3.7 ps, respectively. The slow part corresponds to recondensation of QPs into Cooper pairs, whereas the fast component survives even above T_c and was associated to a pseudogap in Refs. [7,9].

The situation for $\mathbf{E} \parallel c$ is yet richer in detail. While all essential features discussed in the following are also evident in $\Delta\sigma_1(\omega, \tau)$, the 2D map of the absorption coefficient $\Delta\alpha(\omega, \tau)$ illustrates the pump-probe dynamics most obviously [Fig. 2(b)]: Besides a broadband QP contribution featuring a similar spectral profile as in the case of $\mathbf{E} \perp c$, two narrow minima are superimposed at energies of 38 and 72 meV. These are the fingerprints of pump-induced anomalies of the phonon resonances. Remarkably, the various contributions to the total response follow clearly different dynamics: The spectral weight of the QPs integrated in the energy range from 45 to 60 meV, i.e., between

the phonon resonances, shows the same temporal trace as the in-plane conductivity [Fig. 2(d)]. In contrast, the pump-induced changes of the phonons are delayed. The most striking difference is imprinted on the apex phonon, which exhibits its maximum anomaly as late as 1 ps after photoexcitation [Fig. 2(b)].

Going beyond this qualitative observation, we introduce a line shape analysis of the apex mode which will allow us to single out the microscopic mechanisms underlying the pump-induced phonon anomaly. Figure 3 depicts selected spectra of the real and imaginary parts of the c -axis conductivity in the vicinity of the apex mode. Below T_c , $\sigma_1(\omega)$ features a characteristic asymmetric resonance. We describe the infrared response as the sum of a broadband electronic conductivity $\tilde{\sigma}_{el}(\omega)$ and a phenomenological model [28] of the phonon resonance:

$$\tilde{\sigma}(\omega) = \tilde{\sigma}_{el}(\omega) - \epsilon_0 S \frac{(\omega A + i\omega_0^2)\omega}{\omega_0^2 - \omega^2 - i\omega\gamma}. \quad (1)$$

The phonon contribution is defined by the oscillator strength S , the eigenfrequency ω_0 , and the damping constant γ . The parameter A accounts for the peculiar asymmetry of the line shape below T_c . In order to reduce the number of free parameters, the QP background $\tilde{\sigma}_{el}(\omega)$ may be expressed by a linear function of frequency. Also, the damping $\gamma = 2\pi \times 0.5$ THz is found to be almost temperature-independent. The requirement to reproduce both real and imaginary parts of the spectra simultaneously imposes strict boundaries on the three remaining fit parameters S , ω_0 , and A . As seen in Fig. 3(a) and 3(b), the midinfrared response of YBCO in thermal equilibrium can be described convincingly with Eq. (1).

Figure 4(a) and 4(b) displays the resulting fit parameters A and ω_0 as a function of temperature. The asymmetry sharply decreases upon heating towards T_c and levels off

above this temperature. The physical origin of this phenomenon is explained by the coupling between optical phonons and the Josephson plasmon [24]. In the SC state the Josephson resonance renormalizes the phonon parameters by modifying local fields. In the case of the apex mode, the dominant effect is a strong increase of the asymmetry parameter which, thus, quantifies the coupling of this mode to the Josephson plasmon and scales with the density of the SC condensate. The eigenfrequency ω_0 , on the other hand, shows a continuous redshift with increasing temperature [Fig. 4(b)]. This feature is characteristic of an anharmonic lattice potential, which softens for larger vibrational amplitudes. Consequently, the frequency shift of the apex phonon may be exploited as a sensitive probe of the vibrational occupation.

This idea opens up fascinating new perspectives in combination with ultrafast nonequilibrium measurements: Because of the excellent spectral resolution of our 2D multi-THz data, the model function of Eq. (1) can be numerically adapted to the transient conductivity spectra with high confidence as exemplified in Fig. 3(c) and 3(d). The dynamics of the phonon parameters is, thus, mapped out on a femtosecond scale [Fig. 4(c) and 4(d)]. Starting from the SC state [blue dots in Fig. 4(c)], the asymmetry of the apex mode decreases within $\tau \leq 150$ fs, mimicking the trace of condensate depletion. Analogously, the relaxation to the initial line shape asymmetry follows the QP recombination with a typical time constant of about 4 ps, confirming phonon-plasmon coupling as the microscopic origin of the asymmetry. Note that, unlike thermal activation above T_c , ultrafast optical excitation suppresses the asymmetry entirely for $\tau < 1$ ps. This fact represents a clear manifestation of the extremely nonequilibrium state of the system at early delay times.

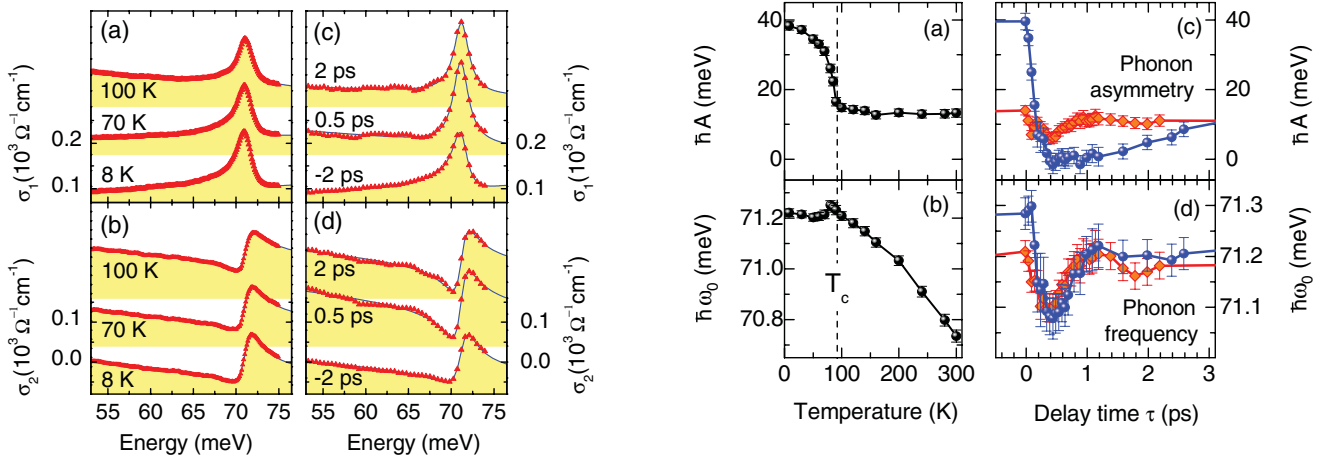


FIG. 3 (color). Spectra of the optical conductivity $\sigma_1(\omega)$ and $\sigma_2(\omega)$ of YBCO for $E \parallel c$: (a),(b) Equilibrium spectra at selected temperatures; (c),(d) transient spectra at selected pump-probe delay times τ measured at $T = 20$ K with $\Phi = 0.3$ mJ/cm². The solid lines show the fitting curves according to Eq. (1).

FIG. 4 (color). (a) Asymmetry factor and (b) eigenfrequency of the apex mode as functions of temperature. (c),(d) The corresponding quantities as functions of the pump-probe delay time τ . The blue dots and red diamonds denote excitations of the SC ($T = 20$ K) and normal state ($T = 100$ K), respectively. The error bars indicate 95% confidence intervals for the fitting parameters.

Remarkably, the eigenfrequency of the apex mode [blue dots in Fig. 4(d)] experiences an abrupt redshift within 150 fs after photoexcitation, i.e., during the onset of the electronic response, and reaches its extremum within 300 fs. The maximum photoinduced softening of the lattice resonance is comparable to the effect induced by a thermal phonon population at $T \approx 200$ K. We thus infer that the optical pump causes a hot phonon population of the apex mode. Subsequently, ω_0 relaxes to a value which is slightly reduced with respect to the equilibrium level at $T = 20$ K. The relaxation time of 1 ps [see Fig. 4(d)] is substantially faster than the QP condensation, which further confirms that the phonon softening is not governed by the coupling to the Josephson plasmon. We suggest that the rapid recovery of ω_0 is explained by a redistribution of the excess energy by phonon-phonon scattering into the large phase space of the entire Brillouin zone.

The damping of the apex mode corresponds to a phonon lifetime of 2 ps, which exceeds the observed relaxation time significantly. This finding shows that phonon-phonon scattering is faster during the hot nonequilibrium state after photoexcitation as compared to a thermal distribution. Additional evidence for a hot phonon population as the main cause of the redshift of the apex mode is provided by the dynamics in the normal state [red diamonds in Fig. 4(d)], where ω_0 follows a quantitatively similar trace. The asymmetry parameter in the normal state, in contrast, shows a substantially reduced change owing to the absence of a macroscopic condensate [red diamonds in Fig. 4(c)] [29].

Our analysis, thus, allows us to disentangle the femtosecond dynamics of the QPs and specific lattice modes, for the first time. The results clearly indicate that a major portion of the absorbed pump energy is transferred to the phonon subsystem within 150 fs. Further evidence supporting this argumentation comes from an energy balance of the pump-induced transition into the normal state. The energy density of ≈ 10 J/cm³ required to suppress the SC phase optically [17,27] is much higher than the thermodynamically determined condensation energy of 1.2 J/cm³ [30]. Following the lines of Ref. [8], only the phonon subsystem possesses sufficient heat capacity to dissipate the high excess energy of the pump pulse. It is worth comparing this situation with the so-called two- or three-temperature models [12,15], which have been established assuming the electron-phonon scattering rate to be negligible as compared to electron-electron interaction. This hierarchy of scattering processes put forward in the context of normal metals [15] or HTSCs like Bi₂Sr₂CaCu₂O_{8+ δ} [12] does not hold in the case of YBCO where a hot phonon population and pair breaking occur on comparable time scales.

In conclusion, we present the first resonant femtosecond observation of both electronic and phononic degrees of freedom in a HTSC. Recording a photoinduced SC-to-normal transition with few-cycle multi-THz pulses provides qualitatively new insight into the electron-phonon

interaction in YBCO. The lattice absorbs a large portion of the pump energy, while the photoexcited charge carriers thermalize and the condensate is depleted. The results indicate strong electron-phonon scattering and introduce a powerful approach to measure the phonon occupation and the coupling to the SC condensate, on a subcycle temporal scale and in a broad variety of strongly correlated material systems.

We thank W. Kaiser for inspiring discussions. This work has been supported by the Deutsche Forschungsgemeinschaft via the Emmy Noether Program and the Research Unit FOR538 (Er342/3 and Ha2071/3), as well as by the Alexander von Humboldt Foundation. The funding of the work at UniFr by SNF Grants No. 200020-119784 and No. 200020-129484 and at SJTU via SCST and the MOST of China (2006CB601003) and by the Kurt Lion foundation is gratefully acknowledged.

*Corresponding author.

rupert.huber@uni-konstanz.de

- [1] A. Lanzara *et al.*, *Nature (London)* **412**, 510 (2001).
- [2] T. Cuk *et al.*, *Phys. Rev. Lett.* **93**, 117003 (2004).
- [3] H. Iwasawa *et al.*, *Phys. Rev. Lett.* **101**, 157005 (2008).
- [4] D. Reznik *et al.*, *Nature (London)* **440**, 1170 (2006).
- [5] J. Lee *et al.*, *Nature (London)* **442**, 546 (2006).
- [6] M. Opel *et al.*, *Phys. Rev. B* **60**, 9836 (1999).
- [7] J. Demsar *et al.*, *Phys. Rev. Lett.* **82**, 4918 (1999).
- [8] P. Kusar *et al.*, *Phys. Rev. Lett.* **101**, 227001 (2008).
- [9] R. A. Kaindl *et al.*, *Science* **287**, 470 (2000).
- [10] R. D. Averitt *et al.*, *Phys. Rev. B* **63**, 140502 (2001).
- [11] R. P. Saichu *et al.*, *Phys. Rev. Lett.* **102**, 177004 (2009).
- [12] L. Perfetti *et al.*, *Phys. Rev. Lett.* **99**, 197001 (2007).
- [13] N. Gedik *et al.*, *Science* **316**, 425 (2007).
- [14] V. V. Kabanov *et al.*, *Phys. Rev. B* **78**, 174514 (2008).
- [15] P. B. Allen, *Phys. Rev. Lett.* **59**, 1460 (1987).
- [16] Key findings are also reproduced on YBCO thin films.
- [17] See supplementary material at <http://link.aps.org/supplemental/10.1103/PhysRevLett.105.067001>.
- [18] C. Bernhard *et al.*, *Thin Solid Films* **455**, 143 (2004).
- [19] D. N. Basov *et al.*, *Rev. Mod. Phys.* **77**, 721 (2005).
- [20] F. E. Bates, *Phys. Rev. B* **39**, 322 (1989).
- [21] A. Litvinchuk *et al.*, *Solid State Commun.* **83**, 343 (1992).
- [22] J. Schützmann *et al.*, *Phys. Rev. B* **52**, 13 665 (1995).
- [23] C. Bernhard *et al.*, *Phys. Rev. B* **61**, 618 (2000).
- [24] D. Munzar *et al.*, *Solid State Commun.* **112**, 365 (1999).
- [25] R. Huber *et al.*, *Nature (London)* **414**, 286 (2001).
- [26] C. Kübler *et al.*, *Phys. Rev. Lett.* **99**, 116401 (2007).
- [27] The saturation fluence for the studied YBCO sample is 0.1 mJ/cm².
- [28] J. Humlíček *et al.*, *Phys. Rev. B* **61**, 14 554 (2000).
- [29] The excitation dynamics of the bond-bending vibration suggests a notable anharmonic redshift, as well. However, the analysis is not as clear since the strong influence of the Josephson plasmon inhibits a complete separation of the anharmonic shift; see [17].
- [30] J. W. Loram *et al.*, *Phys. Rev. Lett.* **71**, 1740 (1993).